



Contents

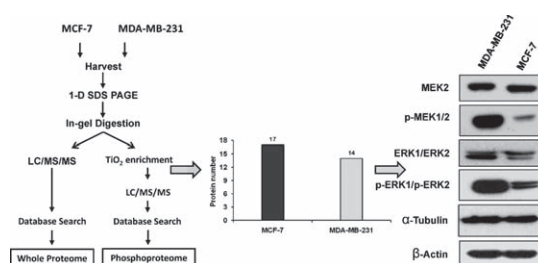
Regular articles

1–12

Comparative phosphoproteome analysis reveals more ERK activation in MDA-MB-231 than in MCF-7

Mohammad Humayun Kabir, Eui Jin Suh, Cheolju Lee

► We analyzed phosphoproteome from two breast cancer cell lines MCF-7 and MDA-MB-231 by mass spectrometry. ► ERK1/ERK2 kinase substrate motif is enriched in MDA-MB-231 compared to MCF-7. ► Differences in phosphoprotein level between MCF-7 and MDA-MB-231 reflect differences in kinase activities as well as protein expression levels. ► Our findings are valuable in breast cancer research due to the wide use of MCF-7 and MDA-MB-231.

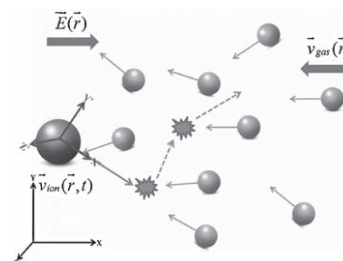


13–21

Computational fluid dynamics-Monte Carlo method for calculation of the ion trajectories and applications in ion mobility spectrometry

Fenglei Han, Yongzhai Du, Shasha Cheng, Qinghua Zhou, Chuang Chen, Keyong Hou, Weiguo Wang, Haiyang Li

► A simulation model for ion motion at atmospheric pressure was built. ► This model considers both electric field and flow field effects. ► This model combines the computational fluid dynamics and Monte Carlo method. ► Ion trajectories and spectrum in the devices can be seen intuitively with this model.

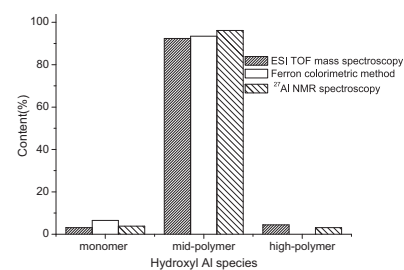


22–29

Quantification analysis of polymeric Al species in solutions with electrospray ionization time-of-flight mass spectrometry (ESI-TOF-MS)

Chenghong Feng, Zhe Bi, Shou Zhao, Ning Li, Dongsheng Wang, Hongxiao Tang

► Quantification analysis method of ESI-TOF-MS on Al speciation was developed and proved to be feasible. ► Keggin-Al₁₃ and mononuclear Al species were proved to be the dominant component of polymeric Al solutions. ► Mass spectrometry provides more information on Al species than ²⁷Al NMR spectroscopy and Ferron colorimetric method.

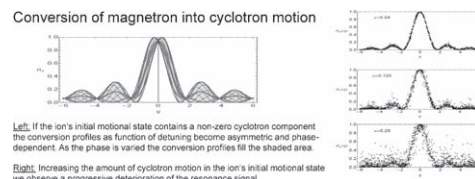


30–38

On the phase dependence of the interconversion of the motional modes in a Penning trap by quadrupolar excitation

Martin Kretzschmar

► Quadrupolar rf-fields with a frequency near the cyclotron frequency ω_c convert magnetron motion into cyclotron motion. ► Starting from pure magnetron motion one obtains symmetric and phase-independent conversion profiles. ► With a non-zero cyclotron component in the initial motional state conversion profiles become asymmetric and phase dependent. ► However, conversion profiles averaged over the phase parameter are symmetric about ω_c . ► Conversion profiles become increasingly fuzzy as the initial cyclotron component increases.

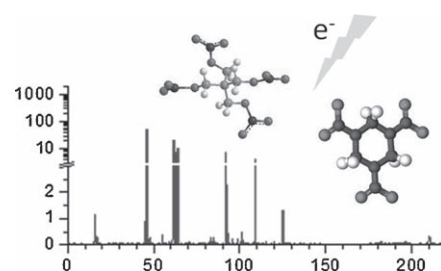


39–43

Semtex 1A and H negative ion resonances for explosives' detection

F. Ferreira da Silva, P. Sulzer, S. Denifl, T.D. Märk, P. Limão-Vieira, P. Scheier

► We present the results obtained in dissociative electron attachment to Semtex in the gas phase by making use of a crossed electron-molecular beam experiment. ► Anion efficiency curves have been measured in an electron energy range from 0 to 12 eV with an energy resolution of ~80 meV.

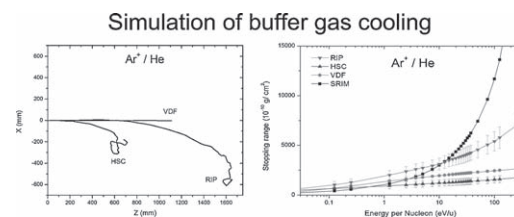


44–48

Energy limitation for models to simulate the buffer gas cooling

Z.C. Zhu, W.X. Huang, Y.L. Sun, Y. Wang, Y.L. Tian, J.Y. Wang

► Viscous damping force (VDF) model, hard sphere collision (HSC) model, and realistic interaction potential (RIP) model. ► The VDF and HSC models are better in low energy range, but the RIP model is better in relatively high energy range. ► In helium buffer gas, the VDF model should be used when the ion's energy is less than ~5 eV/u, and the RIP model less than ~80 eV/u. Above this energy, all three models cannot be used. ► If the buffer gas becomes heavier, the upper limits to use the models decrease.

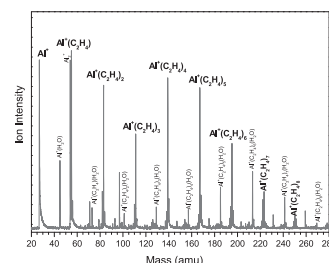


49–55

Structures of $\text{Al}^+(\text{C}_2\text{H}_4)_n$ clusters: Mass-selected photodissociation and *ab initio* calculations

Jinyun Yuan, Yuchao Zhao, Gaolei Hou, Zhen Gao, Weijun Zheng

► We propose that Al-C σ -bonds can be formed in $\text{Al}^+(\text{C}_2\text{H}_4)_n$ ($n > 1$) clusters. ► The strong interaction between Al^+ and ethene molecules weakens the C=C bond significantly. ► Al^+ can trigger addition reaction of ethene molecules to develop chain or ring structures.

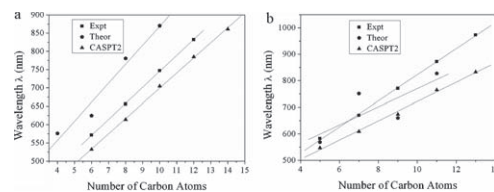


56–62

Theoretical studies on structures and electronic spectra of linear HC_nN^+ ($n = 2-14$)

Yanxin Zhang, Jia Guo, Jinglai Zhang

► Properties of ground- and excited-states for HC_nN^+ ($n = 2-14$) are discussed. ► Odd- n clusters are more stable than even- n analogues with the parity alternation. ► The CASPT2 predicted vertical excitation energies agree well with observed values. ► Notably linear $\lambda-n$ relationships are found in the $(2, 3)^2[\pi \leftarrow X^2]$ transitions.

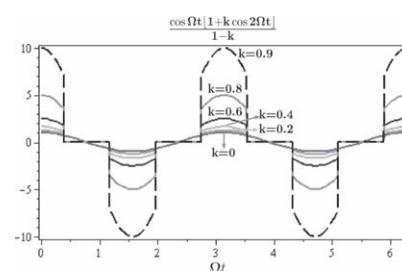


63–69

A new impulsional potential for a Paul ion trap

S. Seddighi Chaharborj, S.M. Sadat Kiai, M.R. Abu Bakar, I. Ziaeiian, I. Fudziah

► We study the dynamical behavior of an ion confined in a Paul ion trap supplied with a new periodic impulsional potential form. ► We used fifth order Runge–Kutta method to compute the accurate stability diagrams. ► For given operational parameters such as $\Omega = 2\pi \times 1.05 \times 10^6 \text{ rad s}^{-1}$, $z_0 = 0.783 \text{ cm}$, and rf only mode $U = 0$ ($a_z = 0$), the potential difference V_{rf} values for $m = 1$ and $m = 2$ ions is found to be $V_{rf} = 11 \text{ V}$ for $k = 0$ and $V_{rf} = 130 \text{ V}$ for $k = 0.9$.

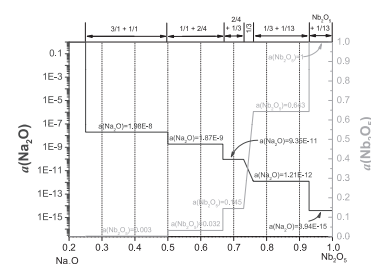


70–78

Knudsen effusion mass spectrometric approach to the thermodynamics of $\text{Na}_2\text{O-Nb}_2\text{O}_5$ system

A. Popovič, L. Bencze, J. Koruza, B. Malič, M. Kosec

► We measure activity of Na_2O and Nb_2O_5 in two-phase regions of $\text{Na}_2\text{O-Nb}_2\text{O}_5$ system. ► We determine Gibbs energy of formation and enthalpy of formation of five phases of $\text{Na}_2\text{O-Nb}_2\text{O}_5$ system. ► We find that NaNb_3O_8 is thermodynamically stable against decomposition also below 950 K.

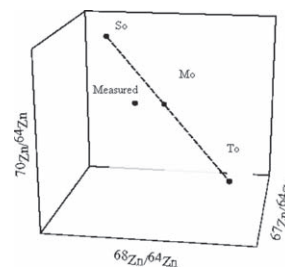


79–87

Zinc isotope fractionation analyses by thermal ionization mass spectrometry and a double spiking technique

Osama Y. Ghidan, Robert D. Loss

► The first identification of δZn in terrestrial materials by TIMS-double spiking. ► Procedures to solve analytical issues involved in TIMS-Zn isotope analysis.

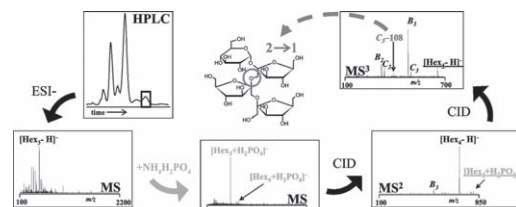


88–96

Analysis of free oligosaccharides by negative-ion electrospray ion trap tandem mass spectrometry in the presence of H_2PO_4^- anions

Ivo Fabrik, Richard Čmelík, Janette Bobál'ová

► Addition of $\text{NH}_4\text{H}_2\text{PO}_4$ increases the sensitivity of negative-ion MS of oligosaccharides. ► $\text{NH}_4\text{H}_2\text{PO}_4$ clusters indicate high amounts of salt. ► Adduct-derived cross-ring fragments appeared during fragmentation. ► Dextrins, fructans and raffinose oligosaccharides were identified in plant samples.

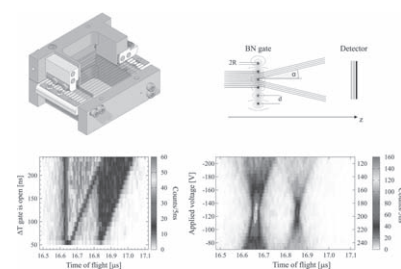


97–103

A large Bradbury Nielsen ion gate with flexible wire spacing based on photo-etched stainless steel grids and its characterization applying symmetric and asymmetric potentials

T. Brunner, A.R. Mueller, K. O'Sullivan, M.C. Simon, M. Kossick, S. Ettenauer, A.T. Gallant, E. Mané, D. Bishop, M. Good, G. Gratta, J. Dilling

► We present a new and simple design of a UHV compatible Bradbury Nielsen ion gate. ► The gate design is based on two photo-etched wire grids allowing exible wire spacing and large area. ► Such a Bradbury Nielsen gate was systematically tested at the TITAN experimental facility and has been used during the Penning trap mass measurement of radioactive Rb. ► An asymmetric voltage applied to the gate results in a change of the ions' time-focus. Based on this, the time resolution of the gate can be improved at the cost of energy spread.

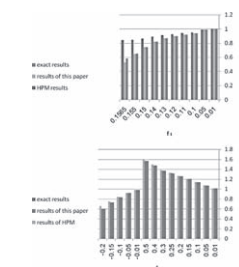


104–108

Calculation of secular axial frequencies in a nonlinear ion trap with hexapole, octopole and decapole superpositions by a modified Lindstedt–Poincare method

Alireza Doroudi, Amineh Rezaeian Asl

► The secular frequencies of a nonlinear ion trap are studied. ► The hexapole, octopole and decapole superpositions are considered. ► The modified Lindstedt–Poincare method is used. ► The secular frequencies of the nonlinear ion trap are calculated by this method. ► The calculated results are compared with the results of homotopy perturbation method and the exact results.

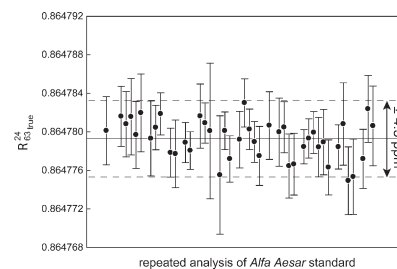


109–117

High precision tungsten isotope measurement by thermal ionization mass spectrometry

Mathieu Touboul, Richard J. Walker

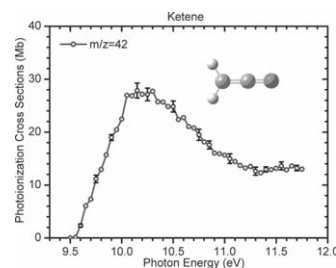
► We present a new high precision $^{182}\text{W}/^{184}\text{W}$ measurement protocol by N-TIMS. ► Instrumental mass fractionation requires correction using a double normalization procedure. ► This procedure allows correction of isotope fractionation for both, tungsten and oxygen. ► This method permits an external reproducibility of <5 ppm for natural samples.



118–128**Absolute photoionization cross-sections of some combustion intermediates**

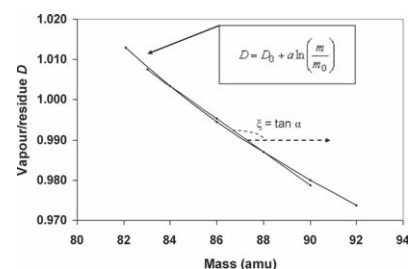
Bin Yang, Juan Wang, Terrill A. Cool, Nils Hansen, Scott Skeen, David L. Osborn

- Absolute photoionization cross-sections for 30 combustion intermediates.
- Updated accurate cross-sections for allene.
- First measurement of the cross-sections for ketene.

**129–132****Distillation law and exponential model of isotope fractionation**

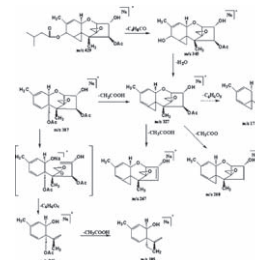
Giancarlo Cavazzini

- The exponential law of isotope fractionation is modelled in terms of distillation law.
- The relationship between distribution coefficient and isotope mass is found.
- The distribution coefficient is a natural logarithmic function of isotope mass.

**133–140****Fragmentation study of five trichothecenes using electrospray hybrid ion trap/time-of-flight mass spectrometry with accurate mass measurements**

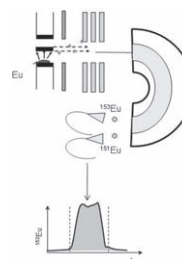
Zhao-Ying Liu, Chun-Hong Yu, Leren Wan, Zhi-Liang Sun

- The fragmentation pathways for five trichothecenes are proposed.
- Eliminations of isovaleryloxy group and acetic acid were the common fragmentation pathways of T-2 toxin and HT-2 toxin.
- The cleavage of epoxy was the common fragmentation pathways of DON, 3-AcDON and NIV.

**141–147****The use of total evaporation method using Channeltron electron multipliers by thermal ionization mass spectrometry for europium isotope ratio measurements on picogram sample amounts**

S. Mialle, A. Quémet, A. Ponvienne, A. Gourgiotis, M. Aubert, H. Isnard, F. Chartier

- Total Flash Evaporation method was tested in multistatic collection mode on Channeltron detectors, reducing the amounts of samples deposited on the filament.
- In order to obtain accurate isotope results, intrinsic parameters such as applied voltages, dead time and noise were determined.
- A Channeltron specific intercalibration gain method was also developed, as this parameter was found to be the major source of uncertainties using this type of detectors.

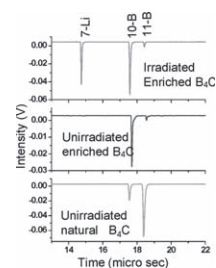


148–153

Quasi-non-destructive isotopic ratio measurement of boron in irradiated control rod B₄C pellets using a home-built reflectron time-of-flight mass spectrometer

P. Manoravi, M. Joseph, N. Sivakumar, P.R. Vasudeva Rao

► Laser mass spectrometry studies on B₄C control rod pellets. ► Boron isotopic analysis in irradiated control rod pellets of FBTR. ► Burn-up of Boron-10 in B₄C pellets used in fast reactor core.

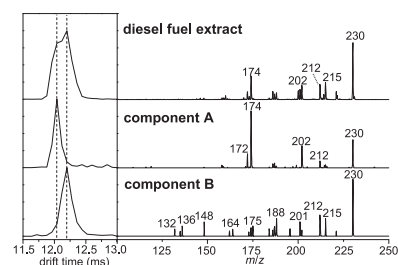


154–160

Extracted fragment ion mobility distributions: A new method for complex mixture analysis

Sunyoung Lee, Zhiyu Li, Stephen J. Valentine, Steven M. Zucker, Nathaniel Webber, James P. Reilly, David E. Clemmer

► A new method for constructing ion mobility distributions of precursor ions based upon the extraction of drift time distributions is described. ► Extracted fragment ion mobility distributions (XFIDTD) approach is reliable to reveal the mobility distribution of the precursor ion. ► Extraction of data for a single fragment ion is sufficient to distinguish the precursor ion mobility distribution of isobaric, basic components from diesel fuel.

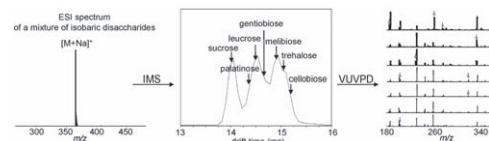


161–167

Analyzing a mixture of disaccharides by IMS-VUVPD-MS

Sunyoung Lee, Stephen J. Valentine, James P. Reilly, David E. Clemmer

► Both CID and VUV photodissociation provide information of linkage type and anomeric configuration of isobaric disaccharides. ► Compared to CID, VUV photodissociation generates additional fragments that are helpful to distinguish each component from a mixture of disaccharide isomers. ► Extracted fragment ion mobility distributions reveal precursor ion mobilities from a mixture.



168–175

Comparative analysis of aromatic diisocyanate conjugation to human albumin utilizing multiplexed tandem mass spectrometry

Justin M. Hettick, Paul D. Siegel

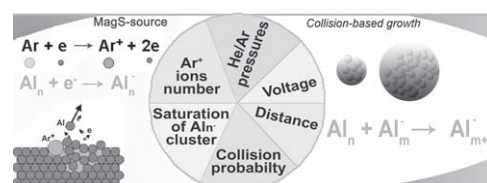
► Sites of diisocyanate–albumin conjugation identified via multiplexed tandem mass spectrometry. ► Conjugation sites identified for toluene diisocyanate and methylene diphenyl diisocyanate. ► Conjugation sites identified at varying mol ratios and in different solvent systems. ► Methylene diphenyl diisocyanate conjugates albumin at a subset of toluene diisocyanate sites. ► Conjugation sites identified may be useful for biomonitoring of exposed diisocyanate workers.



176–181

Growth kinetics of Al clusters in the gas phase produced by a magnetron-sputtering source

Zhixun Luo, W. Hunter Woodward, Jordan C. Smith, A.W. Castleman Jr.

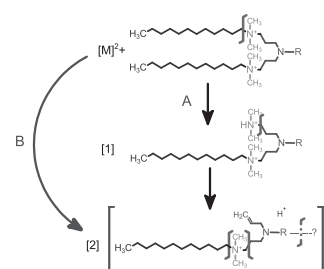


182–191

Mass spectrometric analysis of amino acid/di-peptide modified gemini surfactants used as gene delivery agents: Establishment of a universal mass spectrometric fingerprint

Waleed Mohammed-Saeid, Joshua Buse, Ildiko Badea, Ronald Verrall, Anas El-Aneed

- Evaluation of the tandem mass spectrometric behaviour of novel mono-amino acid/di-peptide gemini surfactants.
- Single stage QqToF-MS in the positive ion mode verified the molecular composition of all tested compound.
- Common fragmentation behaviour among all tested compounds was observed allowing for the establishment of a universal fragmentation pattern.
- The universal fragmentation pattern was confirmed by MS/MS/MS analysis.

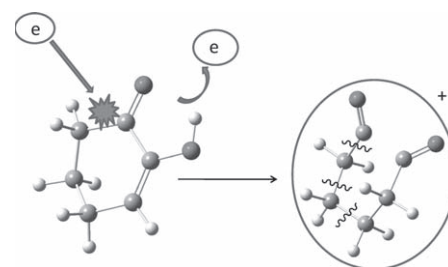


192–199

Electron ionization cross-section and fragmentation of α -cyclohexanedione

Anamika Mukhopadhyay, Arup Kumar Ghosh, Moitrayee Mukherjee, Tapas Chakraborty

- Low-energy electron ionization and fragmentation spectra of α -cyclohexanedione are measured.
- Fragmentation channels are correlated with the calculated thermodynamic parameters.
- Ionization cross-sections of the molecule are measured for different electron kinetic energies.

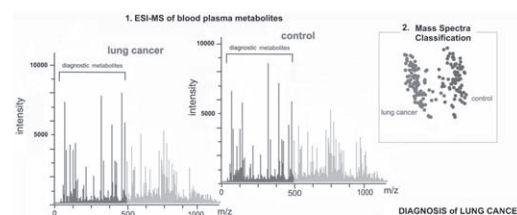


200–205

Diagnosis of lung cancer based on direct-infusion electrospray mass spectrometry of blood plasma metabolites

Petr G. Lokhov, Oleg N. Kharybin, Alexander I. Archakov

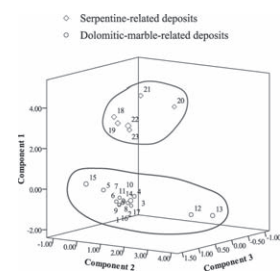
- Diagnostic power of blood plasma metabolites was investigated.
- Blood plasma metabolites were analyzed using direct-infusion ESI mass spectrometry.
- Mass spectra were used for samples classification.
- Accuracy of classification of lung cancer samples was 93.3% (sensitivity 94.1%, selectivity 92.4%).



206–211**Glow discharge mass spectrometry studies on nephrite minerals formed by different metallogenic mechanisms and geological environments**

Bilige Siqin, Rong Qian, Shangjun Zhuo, Fuxi Gan, Min Dong, Yanfen Hua

► GD-MS analysis was used to study nephrite minerals of different deposits. ► Two types of nephrite minerals were separated by Cr, Co and Ni elements. ► Nephrite minerals from some specific deposits had their typical elements.

**Corrigendum****212–212****Corrigendum to “Calculated electron impact K-shell ionization cross sections for atoms” [Int. J. Mass Spectrom. 269 (2008) 118–130]**

M.R. Talukder, S. Bose, S. Takamura